A novel automated diagnostic system for classification of myocardial infarction ECG signals using an optimal biorthogonal filter bank

Article *in* Computers in Biology and Medicine · July 2018

DOI: 10.1016/j.compbiomed.2018.07.005

CITATIONS
113

READS
1,024

3 authors, including:

Manish Sharma
Institute of Infrastructure Technology Research and Management
100 PUBLICATIONS **3,952** CITATIONS

SEE PROFILE

Ru San Tan
National Heart Centre Singapore
570 PUBLICATIONS **20,759** CITATIONS

SEE PROFILE

A novel automated diagnostic system for classification of myocardial infarction ECG signals using an optimal biorthogonal filter bank

Manish Sharma[a,], Ru San Tan[b], U. Rajendra Acharya[c,d,e]

[a]*Department of Electrical Engineering, Institute of Infrastructure Technology Research and Management, Ahmedabad, India*
[b]*National Heart Centre Singapore, Singapore*
[c]*Department of Electronics and Computer Engineering, Ngee Ann Polytechnic, Singapore 599489, Singapore*
[d]*Department of Biomedical Engineering, School of Science and Technology, SIM University, Singapore.*
[e]*School of Medicine, Faculty of Health and Medical Sciences, Taylor's University, 47500 Subang Jaya, Malaysia*

Abstract

Myocardial infarction (MI), also referred to as heart attack, occurs when there is an interruption of blood flow to parts of the heart, due to the acute rupture of atherosclerotic plaque, which leads to damage of heart muscle. The heart muscle damage produces changes in the recorded surface electrocardiogram (ECG). The identification of MI by visual inspection of the ECG requires expert interpretation, and is difficult as the ECG signal changes associated with MI can be short in duration and low in magnitude. Hence, errors in diagnosis can lead to delay the initiation of appropriate medical treatment. To lessen the burden on doctors, an automated ECG based system can be installed in hospitals to help identify MI changes on ECG. In the proposed study, we develop a single-channel single lead ECG based MI diagnostic system validated using noisy and clean datasets. The raw ECG signals are taken from the Physikalisch-Technische Bundesanstalt database. We design a novel two-band optimal biorthogonal filter bank (FB) for analysis of the ECG signals. We present a method to design a novel class of two-band optimal biorthogonal FB in which not only the product filter but the analysis lowpass filter is also a halfband filter. The filter design problem has been composed as a constrained convex optimization problem in which the objective function is a convex combination of multiple quadratic functions and the regularity and perfect reconstruction conditions are imposed in the form linear equalities. ECG signals are decomposed into six subbands (SBs) using the newly designed wavelet FB. Following to this, discriminating features

*Corresponding author
Email addresses: manishsharma.iitb@gmail.com (Manish Sharma), <tan.ru.san@singhealth.com.sg> (Ru San Tan), aru@np.edu.sg (U. Rajendra Acharya)

namely, fuzzy entropy (FE), signal-fractal-dimensions (SFD), and renyi entropy (RE) are computed from all the six SBs. The features are fed to the k-nearest neighbor (KNN). The proposed system yields an accuracy of 99.62% for the noisy dataset and an accuracy of 99.74% for the clean dataset, using 10-fold cross validation (CV) technique. Our MI identification system is robust and highly accurate. It can thus be installed in clinics for detecting MI.

Keywords: Electrocardiogram, entropy, fractal dimension, optimal biorthogonal filter bank, stopband energy, KNN

---

1. Introduction

Myocardial infarction (MI) occurs when blood flow to an area of the heart muscle (myocardium) is interrupted [1]. These interruption are caused by the blockage of the coronary arteries due to acute rupture of cholesterol-rich atherosclerotic plaques. The affected myocardium stops functioning, and if left untreated, may lead to chronic heart failure [2]. MI is responsible for many deaths around the world. It has been appraised that around 750,000 Americans suffer heart attacks every year [3]. Among these, 210,000 have recurrent heart attacks [3] . It is challenging and essential to detect the initial stage of MI so that early correct treatment can be instituted, which increase life expectancy. A system needs to be designed that is able to diagnose the MI accurately, rapidly and yet is robust.

The ECG is a less expensive technique which is commonly employed for the determination of MI. ECG depicts the electrical functioning of heart [4, 5]. Safdarian et al. [6] achieved an accuracy of 94.74% for detection of MI using ECG beats signals. Lahiri et al [7] employed R-peaks detection method and achieved an accuracy of 90%. The results achieved by Acharya et al. in [8] using single lead and a single signal ECG based model motivated us to employ the same in our work. They achieved the highest accuracy of 95.22% using clean dataset and 93.53% with noisy dataset. The single-channel single-signal based systems are highly desirable because they are convenient, inexpensive, and portable MI diagnostic system. Such systems are essential in practical applications as they can increase the productivity and reduce the cost significantly [9, 10].

A computer-aided diagnosis (CAD) system based on ECG is preferred to classify MI signals as these systems are reliable, fast, accurate and robust compared with conventional methods used in the industry. Several researchers have tried to develop these systems which can be employed for practical usage in the detection of MI ECG signals. Recently, Acharya et al [8] employed 11-layer deep convolution neural network for the diagnosis of MI ECG signals. They performed the classification on both noisy and clean datasets. However, the proposed model is not cost-effective and requires high computational power. Liu et al [11] developed a model based on R-peaks detection and employed polynomial fitting (polyfit). Such models which employ polyfit are mostly overfitted as they involve high degrees of polynomials leading to high fluctuations.

Several CAD MI detection systems have been developed [12, 13, 14, 15, 16, 7, 11, 6, 17, 18], however, their performance have been evaluated using only clean ECG signals. In this paper, we have performed the classification of MI ECG signals considering both clean and noisy ECG datasets using the wavelet-based features obtained from newly designed optimal biorthogonal wavelet filter bank (OBWFB). For the analysis of ECG signals, the OBWFB has been obtained by minimizing a mutiple-objective function that considers passband and stopband errors, time localization and frequency localization. The novelties and merits of the design method are listed below:

1. A time–domain approach has been presented, which does not involve any parametrization and is straightforward. It does not involve the design of kernels (subfilters), the filter coefficients are determined directly. The method provides global solution and does not need any initial guess. The method is a non iterative.
2. Unlike the indirect two-step method of Vaidyanathan and Nguyen [19] to design halfband filters, our method is direct and the coefficients of the halfband analysis filter are obtained in one step.
3. Our method adopts a two stage approach to design FBs, where the optimal analysis filter is obtained first and then the optimal synthesis filter is designed. It provides flexibility to control the attributes of analysis independently and separately.
4. The cost function is a multiple objective function which is convex-quadratic function of the pass-band and stop-band errors, time localization and frequency localization. The desired regularity can be imposed in the form of linear equality constraints. The multi-objective cost function employed by us offers the flexibility to tradeoff between several desired attributes.

For developing an automated MI detection system, we have extracted Renyi entropy (RE), signal fractal dimension (SFD) and fuzzy entropy (FE) of subbands obtained from wavelet decomposition of ECG signals using the aforementioned newly designed wavelet FB. After the extraction of features, each feature's t-value is evaluated using Student's t-test to check the effectiveness of the feature and to reduce the redundancy[20]. After the evaluation, we have used several supervised machine learning (ML) algorithms including k-nearest neighbours (KNN) algorithm for the classification of the features into normal and MI affected ECG signals. The salient features of the proposed model are mentioned below:

- The use of KNN has reduced the computational cost by a significant margin compared to the previous works based on deep learning (DL) algorithms [6, 7, 8] and other ML algorithms like support vector machine (SVM)[18, 17] which have a high computational requirement.

- The proposed model is validated using k-fold cross-validation (CV), which ensures the robustness of the model and reduces chances of over-fitting.

- The proposed CAD has given the highest average accuracy (ACC), sensitivity (SEN) and specificity (SPE) of 99.74%, 99.84% and 99.35% respectively for the classification using clean ECG dataset. The ACC, SEN and SPE of 99.62%, 99.76% and 99.12% respectively were obtained when the classification was performed on raw noisy dataset using 18 differentiating features with KNN classifier.

2. Datasets Used

We have used the *Physikalisch-Technische Bundesanstalt* diagnostic ECG database [21] to obtain the clean ECG signals for the classification of MI signals. The dataset consists of 50728 ECG epochs belonging to 200 subjects, out of which 148 subjects (40182 epochs) were suffering from MI and the rest 52 subjects (10546 epochs) were normal. The sampling rate of 1000 Hz has been chosen to sample ECG signals. Each ECG signal was segmented such that the newly segmented ECG beats consist of 651 samples each. In total, there are 50,728 ECG signals consisting of 40,182 MI affected ECG signals and 10,546 normal ECG signals. In this study, we have performed classification on two datasets - noisy and clean.

Fig. 1 shows a sample ECG signal of normal and MI affected ECG, respectively for both noisy and clean datasets.

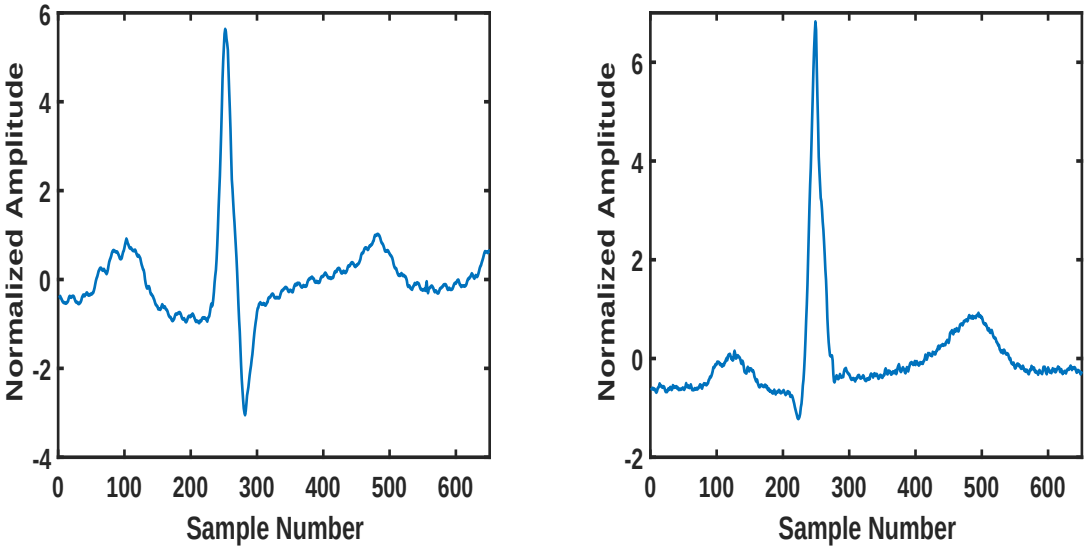

(a) Normal ECG (noisy data)

(b) MI ECG (noisy data)

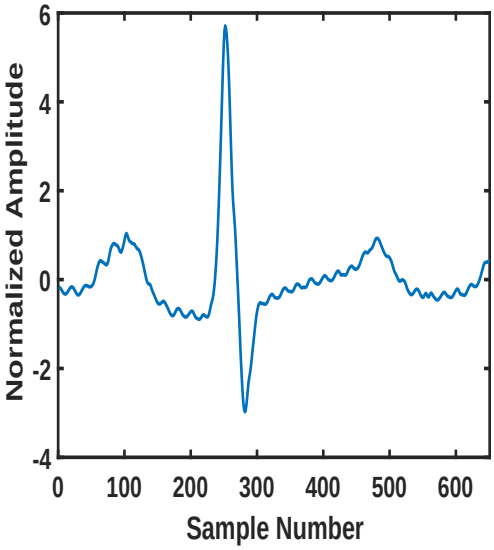

(c) Normal ECG (clean data)

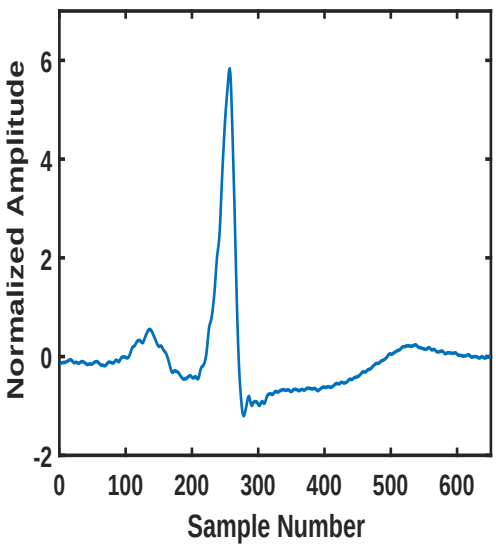

(d) MI ECG (clean data)

Figure 1: Sample ECG signals for both clean and noisy dataset.

3. Methodology

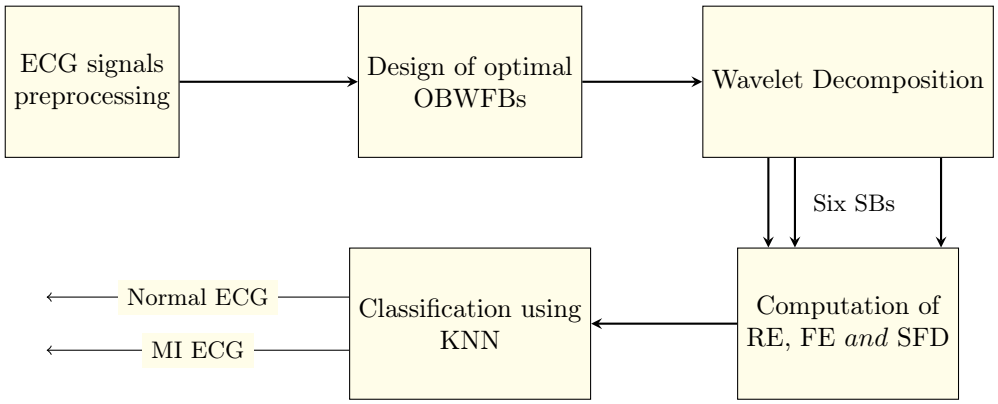

Figure 2: Flow chart showing methodology used for MI ECG signals diagnosis.

3.1. Pre-Processing

The designed model is tested on two datasets of ECG data both involving the same number of ECG beats. One of the datasets employed is noisy (without removal of artifacts) which is referred as Dataset-A. The other dataset used is clean, which is obtained after removal of baseline wander and noise, and it is referred as Dataset-B. The removal of baseline wander, and the noise is done using DB-6 wavelet function [22]. Pan Tompkins algorithm [23] has been used to detect R-peaks from the ECG signal. The detected R-peaks are used for the segmentation of ECG beats (651 samples each). Z-score normalization is performed on every epoch of both the datasets to eradicate the problem of amplitude scaling.

4. The Proposed Optimal Wavelet Filter Bank

Two channel FBs find manifold applications in various fields including image processing, sparse signal processing, signal analysis, communications and design of wavelet bases [24, 25, 26, 27, 28, 29]. The FB design problems can be cast as optimization problems, which may be nonconvex and highly nonlinear [30, 31, 32]. In some cases the perfect reconstruction (PR) condition cannot be satisfied exactly. Another challenge is to control the attributes of the analysis and synthesis filters independently. Moreover, when FBs are used to construct the wavelet bases, they must satisfy certain conditions [33]. As a result, the wavelet FB design problem becomes a highly constrained nonconvex optimization problem. Consequently, globally optimal solutions are not guaranteed, and the computational cost of obtaining a good solution is very high. The design of optimal PR FB that satisfies the desired constraint with low computational

complexity is being investigated. To design the optimal filters, generally, min-max and least square approaches are used.[24] The eigenfilter-based approaches have also been employed. [34, 35, 36].

In wavelet transform or subband coding of a signal, an important issue is the computational cost of filtering involved in the coding. In order to design FBs that offer low computational complexity in the subband coding of a signal, a special class of two channel biorthogonal FBs was introduced by Phoong et al.[37] in which not only the product filter but the analysis low pass filter is also a half band filter. In this technique, which is popularly known as half band pair filter bank (HPFB) technique, first a pair of prototype subfilters (kernels) is designed. Then, the filters are obtained from the lifting of the pair of subfilters. This class is developed to obtain a hierarchical representation of the video signal so that the signal can be compressed at a low bit rate . This class has been found useful in the low bit-rate video compression standard scalable MPEG-2 [38]. The lowpass filters satisfying half band condition are commonly called interpolating filters or à trous filters [39]. These filters are also used in the à trous algorithms to compute samples of CWT quickly. Since, the nearly half of the coefficients of the analysis of lowpass filters are zero valued, it considerably reduces the computational cost of filtering involved in DWT/IDWT. This motivated us to design the special class of optimal biorthohonal filterbanks where the analysis lowpass filter is a halfband filter.

In image coding applications, FBs are generally designed by taking the frequency selectivity and regularity of filters as optimality criteria. However, in certain applications, joint time-frequency localizations of filters play a vital role, and therefore it must be accounted for filter design problems. Wilson and Granlund [40] found that the time-frequency optimized filters are very effective in certain image processing applications. It is observed by Dandach and Siohan [41] that the duration-bandwidth localized FBs work well in lessening interchannel interference and intersymbol interference in case of multicarrier modulations such as OFDM. Further, Monro and Sherlock [42] noticed the excellent performance of joint duration-frequency localized filter in image compression applications. This motivated us to design the optimal FBs where the optimality criterion considers a combination of joint time-frequency localization, frequency selectivity and regularity of the filters.

Though the HPFB technique presented by Phoong et al. [37] offers a structured way to design FB, however, the technique is highly restrictive. There are certain restrictions on the frequency responses of the filters. In order to obtain some control on frequency responses of the filters, Tay [43] combined HPBF design approach and parametrized Bernstein polynomial (PBP), and optimal filters are obtained by searching the two sets of free parameters, iteratively. Similarly, to obtain certain control on joint time-frequency localization of filters. Tay [44] suggested a method combining HPFB technique with PBP. Recently, Baradarani et al. [45] presented a design of half band pair filter banks which provide control between frequency selectivity and regularity. The HPFB design technique [37] is an indirect approach in which two subfilters (kernels) are designed first, and then filters are obtained by lifting the subfilters. Though we

design a class of FBs in which the analysis filter is a halfband filter similar to the class of FB designed by Phoong et al. [37]. However, our design method is quite different from the indirect method of Phoong et al. [37] as well as its variant [45, 44, 43]. Theses indirect methods are restrictive. For instance, the synthesis filter cannot have regularity more than the analysis filters. Our design method is a direct, time domain approach and it does not involve the design of intermediate subfilters (kernels). Also, our method does not involve any parametrization. It does not pose restrictions unlike the existing HPFB techniques and offers more flexibility in shaping the filter attributes. Sharma et al. [36] presented an eigen approach to obtain duration-bandwidth optimized biorthogonal FBs. However, in [36] authors design, lowpass windows instead of the filters as the frequency selectivity (in terms of passband and stopband frequencies and the respective ripples) has not been accounted for in the design problems. Further, the analysis filter has not been constrained to be an interpolating filter. Recently, an indirect approach [46] and some of its variant [47, 48] have been presented to overcome limitations of HPFB technique [37], and to obtain certain control on frequency selectivity and regularity of the filters. In these methods, three optimal subfilters are designed first; then the filters are obtained from the lifting of the subfilters. Due to a highly nonlinear relationship between final filters and subfilters, the method does not necessarily yield optimal analysis and synthesis filters. Thus, one does not have any direct control over the final filters. Moreover, although the methods impose the PR constraints structurally. However, the analysis filters cannot be constrained to be a halfband filter. Besides, the computational cost is also increased as one needs to design three subfilters.

In the proposed method, we design linear phase OBWFBs in which the analysis filter has been constrained to be a halfband filter. We present a simple and efficient design technique to control the frequency selectivity, regularity and the time-frequency localization of the filters, simultaneously. First, we design the halfband analysis lowpass filter (HALF) employing a one-step direct approach unlike the two steps indirect approach of designing the halfband filter, presented by Vaidyanathan and Nguyen [19]. To design the halfband analysis filter a linear constrained convex quadratic optimization problem has been formulated. The objective function employed is a convex combination of time and frequency spreads of the filter and passband and stopband errors. The regularity conditions have been imposed as a group of linear equalities. The optimal filter is obtained as the eigenvector corresponding to the smallest eigenvalue of a positive semidefinite matrix. Having designed the HALF, we design the synthesis lowpass filter(SLPF). The design problem has been cast in a similar manner to that of the analysis lowpass filter except with following variations: (i the synthesis filter cannot be constrained to be a halfband filter. (ii) the PR conditions must be imposed along with the regularity constraints.

5. Background and Preliminaries

Let $H_0(z)$ and $H_1(z)$ be the analysis lowpass and highpass filters, respectively; and $F_0(z)$ and $F_1(z)$ be the synthesis lowpass and highpass filters, respectively in a two channel biorthogonal FB (Fig.3).

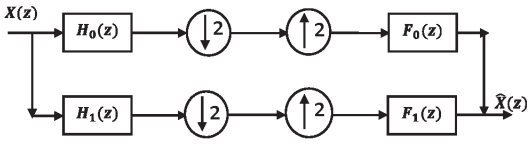

Figure 3: Typical two-band PR filter bank.

The following conditions ensure perfect reconstruction (PR):

$$F_0(z)H_0(-z) + F_1(z)H_1(-z) = 0 \tag{1}$$

$$F_0(z)H_0(z) + F_1H_1(z)(z) = 2z^{-k},\ k \in \mathbb{Z} \tag{2}$$

Defining the product filter as

$$P(z) = z^k H_0(z)F_0(z) \tag{3}$$

The aforementioned PR conditions (1) and (2) can be amalgamated as

$$P(z) + P(-z) = 2 \tag{4}$$

The product filter $P(z)$ satisfying (4) is known as the halfband filter. In time domain, the halfband filter $P(z)$ satisfies the following condition

$$p(2n) = \delta(n) \tag{5}$$

6. Proposed Method

Let $h_0(n)$ and $f_0(n)$ be the impulse response sequences of the HLPF and SLPF the two-channel OBWFB. Let $h(n)$ be the impulse response of a type-1 linear (zero) phase lowpass FIR filter with the length $2N+1$ such that $h(n) \neq 0$ for $-N \leq n \leq N$. In this section, the $h(n)$ represents the impluse response of either the analysis filter $h_0(n)$ or the synthesis filter $f_0(n)$. The frequency-response $H(\omega)$ of the filter $h(n)$ can be presented as

$$H(\omega) = h(0) + 2\sum_{n=1}^{+N} h(n)\cos(\omega n) \tag{6}$$

6.1. Objective Function

In order to formulate optimization problems to design optimal filters of the OBWFB, we define the following objective function, assuming the the energy of the filter $h(n)$ to be unity.

$$\phi = \alpha_1\sigma_n^2 + \alpha_2\sigma_\omega^2 + \alpha_3 E_p + \alpha_4 E_s \tag{7}$$

where, σ_n^2 and σ_ω^2 are time and frequency variances of the filter with unit energy given by [49],

$$\sigma_n^2 = \sum_{n=-\infty}^{\infty} n^2|h(n)|^2 = \frac{1}{\pi}\int_0^\pi \left|\frac{d}{d\omega}\mathbf{H}(\omega)\right|^2 d\omega \tag{8}$$

$$\sigma_\omega^2 = \frac{1}{\pi}\int_0^\pi \omega^2|H(\omega)|^2 d\omega \tag{9}$$

The E_p and E_s are the passband and stop band error between the ideal and the desired frequency responses of the filter given by [19],

$$E_p = \frac{1}{\pi}\int_0^{\omega_p} |H(0) - H(\omega)|^2 d\omega \tag{10}$$

$$E_s = \frac{1}{\pi}\int_0^{\omega_p} |H(\omega)|^2 d\omega \tag{11}$$

where, ω_p and ω_s are the passband edge and stopband edge frequencies, respectively.
By defining the following $(N+1)\times 1$vectors;

$$\mathbf{a} = \begin{bmatrix} h(0) & \sqrt{2}h(1) & \dots & \sqrt{2}h(N) \end{bmatrix}^T \tag{12}$$

$$\mathbf{c}(\omega) = \begin{bmatrix} 1 & \sqrt{2}\cos(\omega) & \dots & \sqrt{2}N\cos(N\omega) \end{bmatrix}^T \tag{13}$$

$$\mathbf{f}(\omega) = \begin{bmatrix} 0 & -\sqrt{2}\sin(\omega) & \dots & -\sqrt{2}N\sin(N\omega) \end{bmatrix}^T \tag{14}$$

The time and frequency variances and passband and stopband errors can be expressed as,

$$\sigma_n^2 = \mathbf{a^T}\left\{\int_\mathbf{0}^\pi \mathbf{f}(\omega)\mathbf{f^T}(\omega)\frac{\mathbf{d}\omega}{\pi}\right\}\mathbf{a} = \mathbf{a^T T a} \tag{15}$$

$$\sigma_\omega^2 = \mathbf{a^T}\left\{\int_\mathbf{0}^\pi \omega^\mathbf{2}\mathbf{c}(\omega)\mathbf{c^T}(\omega)\frac{\mathbf{d}\omega}{\pi}\right\}\mathbf{a} = \mathbf{a^T F a} \tag{16}$$

$$E_s = \mathbf{a^T}\left\{\int_{\omega_s}^{\pi} \mathbf{c}(\omega)\mathbf{c^T}(\omega)\frac{\mathbf{d}\omega}{\pi}\right\}\mathbf{a} = \mathbf{a}^T\mathbf{S}\mathbf{a} \tag{17}$$

$$E_p = \mathbf{a^T}\left\{\int_{\mathbf{0}}^{\omega_\mathbf{p}} [\mathbf{c}(\mathbf{0}) - \mathbf{c}(\omega)][\mathbf{c}(\mathbf{0}) - \mathbf{c}(\omega)]^\mathbf{T}\frac{\mathbf{d}\omega}{\pi}\right\}\mathbf{a} = \mathbf{a}^T\mathbf{P}\mathbf{a} \tag{18}$$

Thus, the objective function defined in (7) can be expressed as;

$$\phi = \mathbf{a}^T\left\{\alpha_1\mathbf{T} + \alpha_2\mathbf{F} + \alpha_3\mathbf{P} + \alpha_4\mathbf{S}\right\}\mathbf{a} = \mathbf{a}^T\mathbf{R}\mathbf{a} \tag{19}$$

where, $\left\{\alpha_i \text{ s.t. } 0 \leq \alpha_i \leq 1; \sum \alpha_i = 1\right\}$ are weighting or trade-off factors that provide the trade-off between time and frequency variances as well as passband and stopband errors. The matrices,$\mathbf{T}, \mathbf{F}, \mathbf{P}, \mathbf{S}$ and $\mathbf{R} \in \mathbb{R}^{(N+1)\times(N+1)}$ are positive definite matrices. Hence, it is evident from (19) that the objective function, ϕ, is a convex-quadratic function in optimization variable $\mathbf{a}$. Therefore, the global optimal solution can be obtained.

6.2. Constraints

The filter design problems have been formulated as constrained optimization problems. The regularity, halfband and perfect reconstruction conditions have been imposed as linear equality constraints in the design variables. In the design of a wavelet FB, regularity of the filters is an essential requirement, which is attained by imposing zeros at $z = -1$ in the case of two-band FB. To impose the regularity of order K (i.e. K zeros at $z = -1$), the frequency response $H(\omega)$ should satisfy the following condition:

$$\left.\frac{d^l H(\omega)}{d\omega^l}\right|_{\omega=\pi} = 0,\ l = 0, 1, 2, \cdots K-1. \tag{20}$$

Then the filter is said to be K–regular filter. It is to note, that in case of type-1 filters, the regularity order must be even, i.e $K = 2M$. The regularity condition (20) can be expresses as the group of linear equalities, $\mathbf{A}\mathbf{a} = \mathbf{0}$. The entry corresponding to the $(k,l)^{th}$ element of $\mathbf{A} \in \mathbb{R}^{(N+1)\times M}$ can be given by:

$$[\mathbf{A}]_{k,l} = \begin{cases} 1 & k, l = 0 \\ \sqrt{2}(l)^{2k}(-1)^l & \text{otherwise} \end{cases} \tag{21}$$

In the proposed design the analysis lowpass filter has been constrained to be a halfband filter. If the filter $h(n)$ is a halfband filter then it must satisfy the following condition

$$h(2n) = 0 \text{ except for } n = 0 \tag{22}$$

Then the halfband condition (22) has been formulated as a collection of linear equalities, $\mathbf{B}\mathbf{a} = \mathbf{0}$. where, the matrix $\mathbf{B} \in \mathbb{R}^{(N+1)\times(N-1)/2}$ whose $(k,l)^{th}$ entry

is given as follows:

$$[\mathbf{B}]_{k,l} = \begin{cases} 1/\sqrt{2} & k = 0, 1 \cdots N; l = 2, 4, \cdots (N-1) \\ 0 & \text{otherwise} \end{cases} \tag{23}$$

In the case of a halfband filter, N must be an odd integer. The time-domain formulation of the PR conditions (5) in the form of linear equations has been presented later in this section.

6.3. Filter Design Optimization Problems

Here, we present the optimization strategy to obtain the optimal halfband analysis filter (HALF) and SLPF. Let the lengths of $h_0(n)$ and $f_0(n)$ be $L_A = 2P+1$ and $L_S = 2Q+1$, respectively. We impose the regularity of the order $2M_A$ and $2M_S$ on the filters $h_0(n)$ and $f_0(n)$, respectively. Let $\mathbf{h} \in \mathbb{R}^{(P+1)}$ and $\mathbf{f} \in \mathbb{R}^{(Q+1)}$ be the optimization vectors, as defined in (12), which contain the later half of the filter coefficients for the HALF and SLPF, respectively. To design filter banks, we employ the complementary technique in which the analysis filter is designed first, then we design the complementary synthesis filter. For the HALF the optimization problem can be cast as

$$\begin{aligned} \underset{\mathbf{h}}{\text{minimize}} \quad & \mathbf{h}^T\mathbf{R}\mathbf{h}, \text{ (Cost function as defined in (19))} \\ \text{subject to} \quad & \mathbf{A}\mathbf{h} = 0, \text{ (Regularity constraint)} \\ & \mathbf{B}\mathbf{h} = 0, \text{ (Halfband constraints)} \\ & \mathbf{h}^T\mathbf{h} = 1, \text{ (Unit norm constraint)} \end{aligned} \tag{24}$$

where, the matrices $\mathbf{A} \in \mathbb{R}^{(P+1)\times M_A}$ and $\mathbf{B} \in \mathbb{R}^{(N+1)\times(P-1)/2}$ have been defined in (21) and (23). For the designed HALF $h_0(n)$, the optimization problem for the synthesis filter has been formulated as

$$\begin{aligned} \underset{\mathbf{f}}{\text{minimize}} \quad & \mathbf{f}^T\mathbf{R}\mathbf{f}, \text{ (Cost function as defined in (19))} \\ \text{subject to} \quad & \mathbf{A}\mathbf{f} = 0, \text{ Regularity constraints} \\ & \mathbf{T}\mathbf{f} = 0, \text{ (PR constraints)} \\ & \mathbf{f}^\mathbf{T}\mathbf{f} = 1, \text{ (Unit norm constraint)} \end{aligned} \tag{25}$$

where, the matrix $\mathbf{A} \in \mathbb{R}^{(Q+1)\times M_S}$ has been defined in (21). The matrix $\mathbf{T} \in \mathbb{R}^{(Q+1)\times(P+Q-1)/2}$ is defined in (26). The entry corresponding to the $(k,l)^{th}$ element of $\mathbf{T}$ can be given as

$$[\mathbf{T}]_{k,l} = \begin{cases} h_0[2k+2] & l = 0 \\ h_0[2(k+1)-l] + h_0[2(k+1)+l] & 1 \le l \le Q \end{cases} \tag{26}$$

where $0 \le k \le \frac{P+Q-1}{2}$. It is clear from (25) and (24) that the filter design problems for the HALF as well as the SLPF have been formulated as linearly con-

strained convex-quadratic optimization problems with a single quadratic constraint in optimization variables.

6.4. Design Algorithm

First, we find the optimal HALF by solving the optimization problem (24) then the optimization problem (25) is solved to obtain the optimal SLPF filter. The optimal filters are obtained as the eigenvectors corresponding to the minimum eigen values of the appropriate positive definite matrices. The complete design algorithm to obtain optimal HALF and SLPF of the OBWFB is summarized in table 1.

Table 1: Filter Designing Steps

1.	Choose appropriate filter-length, L_A, the order of regularity, $2M_A$ and values of tradeoff factors α_i, for the HALF $H_0(z)$ and formulate the optimization problem (24)
2.	Combine liner constraints into a single constraint $\mathbf{Ch} = 0$ by augmenting the matrices $\mathbf{A}$ and $\mathbf{B}$ such that $\mathbf{D} = [\mathbf{A}; \mathbf{B}]$
3.	Since, $\mathbf{h}$ is in the null space of $\mathbf{D}$, the vector $\mathbf{h}$ can be expressed as $\mathbf{h} = \mathbf{Ub}$. Note, $\mathbf{U}$ is a rectangular unitary matrix whose columns of build an orthonormal basis for the null space of $\mathbf{D}$, and $\mathbf{b}$ is any random vector.
4.	We can express the objective function in (24) as, $\mathbf{h}^T\mathbf{Rh} = \mathbf{b^T U^T RUb} = \mathbf{b^T Sb}$. Note, $\mathbf{S} = \mathbf{U^T RU}$ is a symmetric matrix.
5.	The optimal $\mathbf{b}$ is acquired as the eigenvector corresponding to the smallest eigenvalue of the matrix $\mathbf{S}$, employing the Rayleigh theorem. The optimal $\mathbf{h}$ can be found using, $\mathbf{h} = \mathbf{Ub}$.
6.	Choose appropriate L_S, $2M_S$ and α_i for the SLPF and formulate the optimization problem (25)
7.	The optimal SLPF can be acquired in the exactly similar manner as that of the HALF, following steps 3-5

6.5. Design Examples

We consider two examples for demonstrating the efficacy of the presented filter design methodology.

Example 1: For the HALF, the specifications are chosen as follows: number of vanishing moments = 4, length = 15, $\omega_p = 0.3801\pi$, $\omega_s = \pi - \omega_p$ (since the filter is a halfband filter), and the weighting factors as $\alpha = 0$, $\beta = 0$ and $\gamma = 0.5$ For SLPF, number of vanishing moments = 4, length = 29, $\omega_p = 0.3375\pi$, $\omega_s = .6713\pi$ and the weighting factors as $\alpha = 0.01$, $\beta = 0.067$ and $\gamma = 0.5$
Example 2: For the HALF as well as the SLPF lengths and VMs, $\omega_p$and ω_p are the same as that of Example-1. The weighting factors for the HALF are chosen as $\alpha = 0.1$, $\beta = 0.9$ and $\gamma = 0$. For SLPF, the weighting factors are $\alpha = 0.4$, $\beta = 0.6$ and $\gamma = 0$.

Fig. 4 and Fig. 5 shows frequency responses of the designed optimal filters for design Example-1. The Fig. 6 and Fig. 7 show frequency responses of the designed optimal filters for design Example-2. Fig. 8 and Fig. 9 show the pole-zero pattern of HALF and SLPF for design Example-1 for Fig. 10 and Fig. 11 show pole-zero patten of the optima HALF and SLPF for design example-2 .

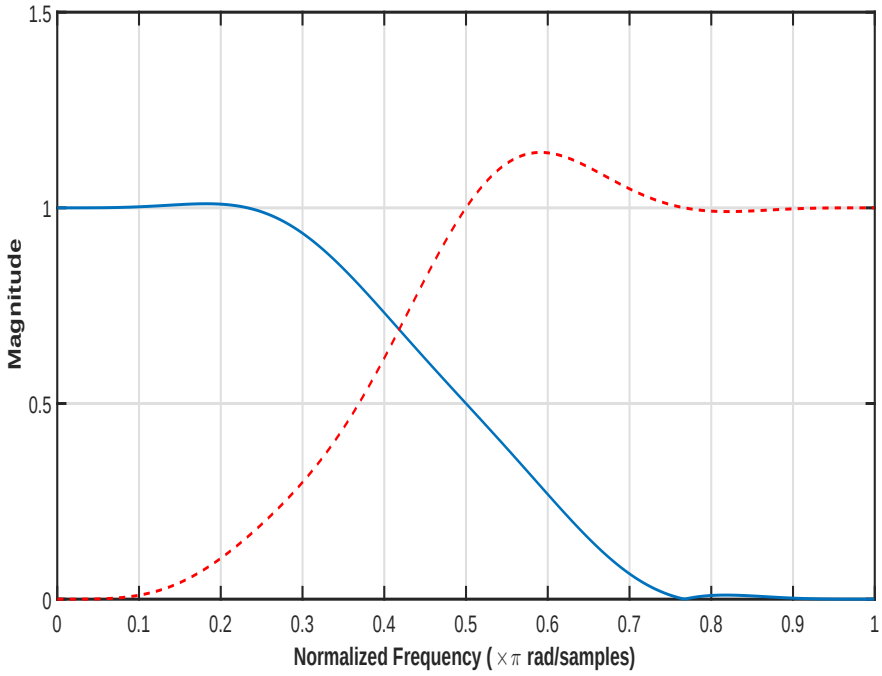

Figure 4: Frequency response of design example-1; —- (solid) denotes HALF, - - - (dashed) denotes analysis highpass filter.

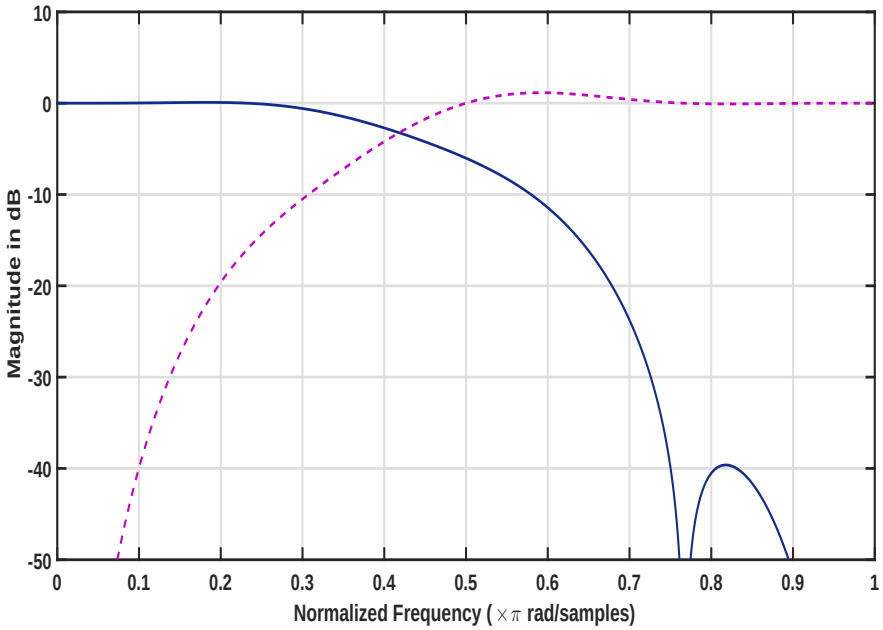

Figure 5: Frequency response (dB) of design example-1; —- (solid) denotes HALF, - - - (dashed) denotes analysis highpass filter.

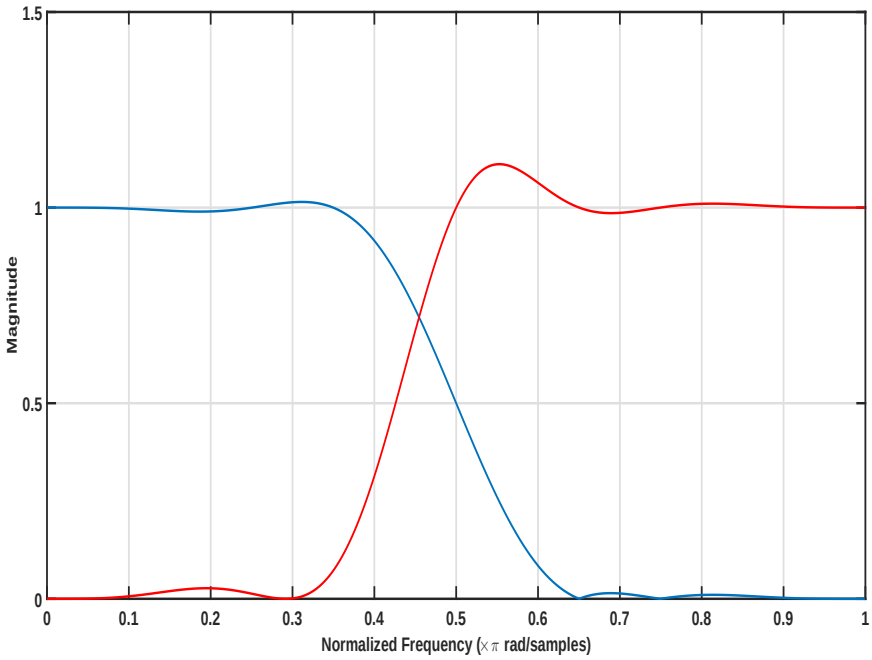

Figure 6: Frequency response of design example-2; —- (solid) denotes HALF, - - - (dashed) denotes analysis highpass filter.

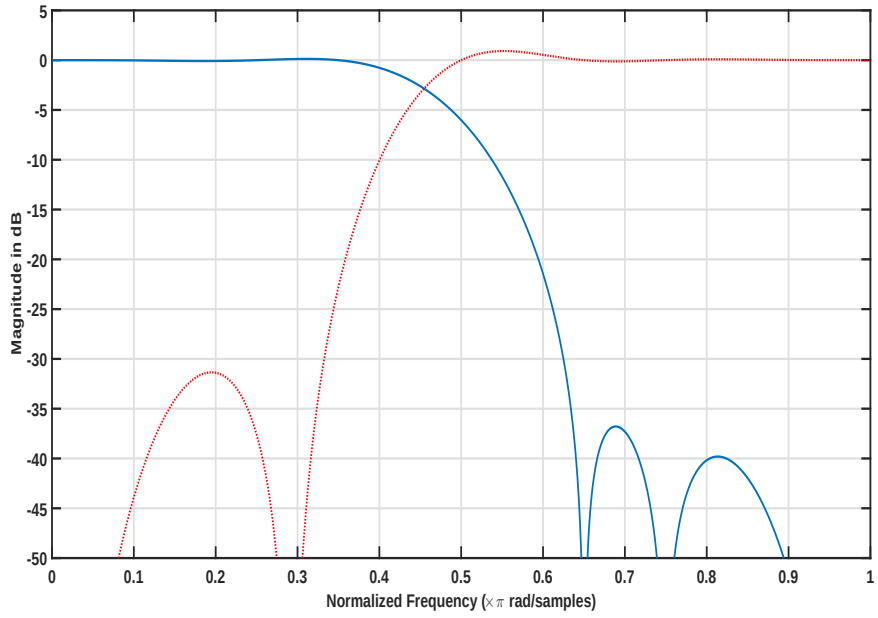

Figure 7: Frequency response (dB) of design example-2; —- (solid) denotes HALF, - - - (dashed) denotes analysis highpass filter.

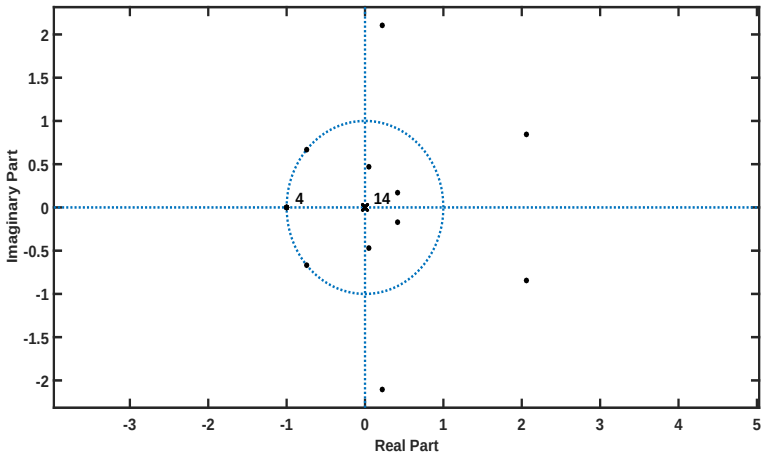

Figure 8: Pole-zero plots for designed optimal HALF (Example 1).

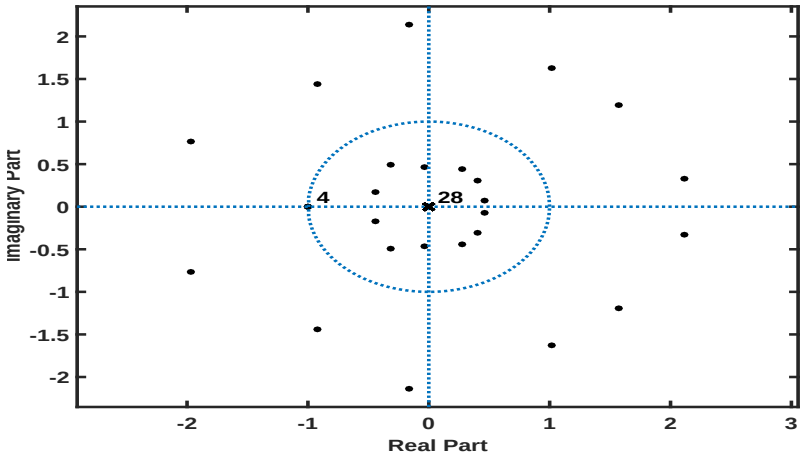

Figure 9: Pole-zero plots for designed optimal SLPF (Example 1).

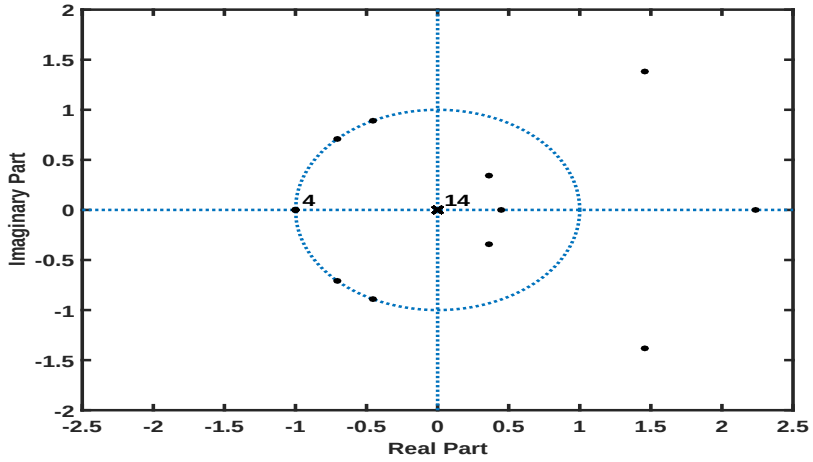

Figure 10: Pole-zero plots for designed optimal HALF (Example 2).

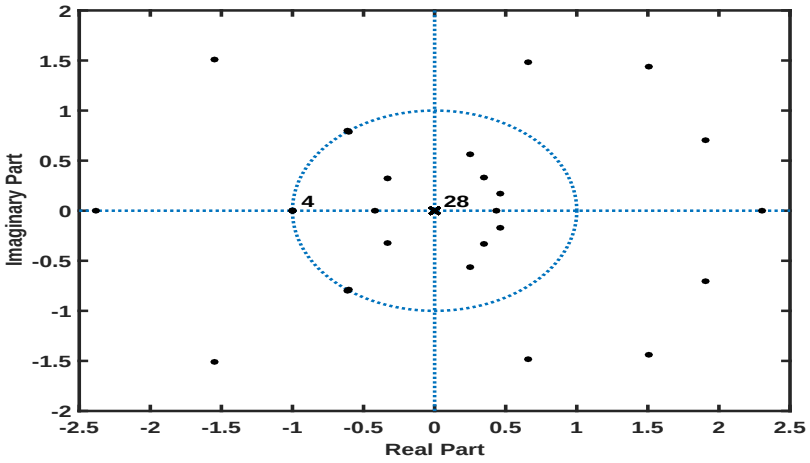

Figure 11: Pole-zero plots for designed optimal SLPF (Example 2).

6.6. Wavelet Decomposition

The ECG signal consists of different frequency components ranging from very low to high frequencies (0 - 50 Hz). It can be noted from the past works [50, 51, 52, 53] that, wavelet decomposition is well suited for non-stationary biomedical signals for achieving good performance. Deciding the level of decomposition is very crucial and important aspect, as it affects the frequency range of SBs and the number of features (NoF) utilized, thereby, affecting the total computational cost required. We have chosen the decomposition level to be 5 so as to retain the dominating frequency components and the most significant SBs. The decomposition yields total six SBs where five are detailed SBs (d1 to d5) and the last one (a5) is regarded as the approximate SB.

Fig. 12 and Fig. 13 shows the SBs of the normal and MI ECG signal, respectively for the Dataset-A. The Fig. 14 and Fig. 15 shows the SBs of the normal and MI ECG signal, respectively for the Dataset-B.

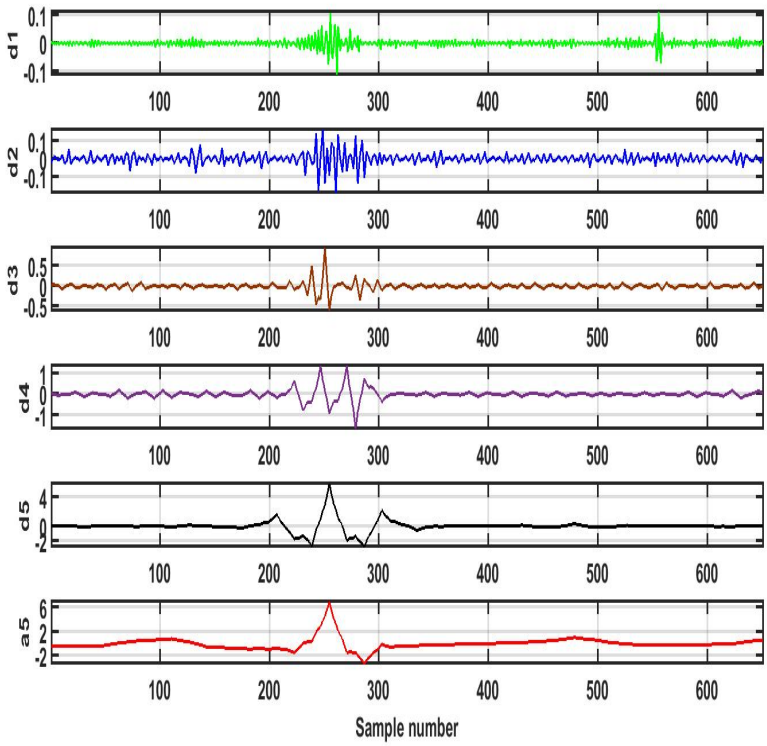

Figure 12: SBs of normal ECG signal (Dataset-A).

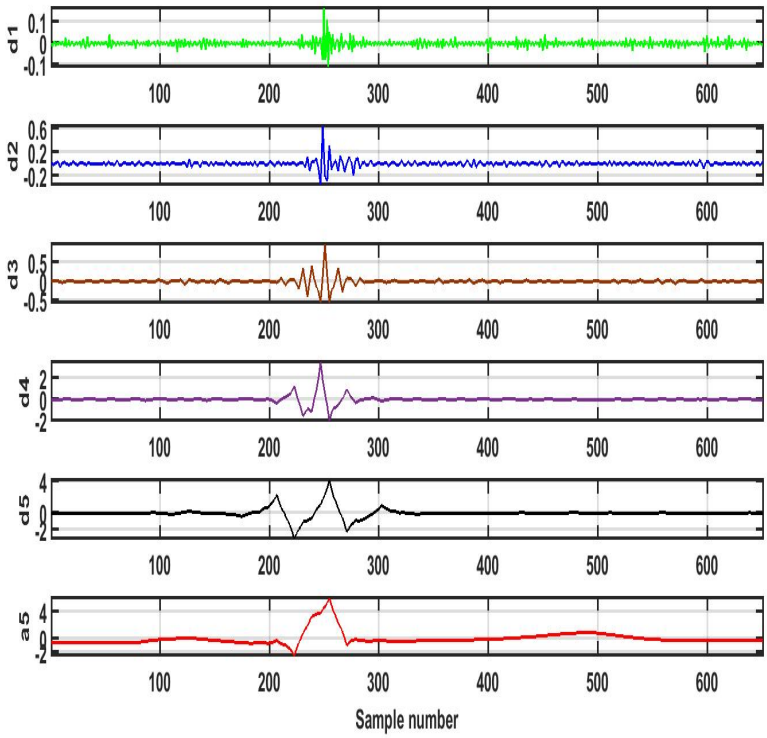

Figure 13: SBs of MI ECG signal (Dataset-A).

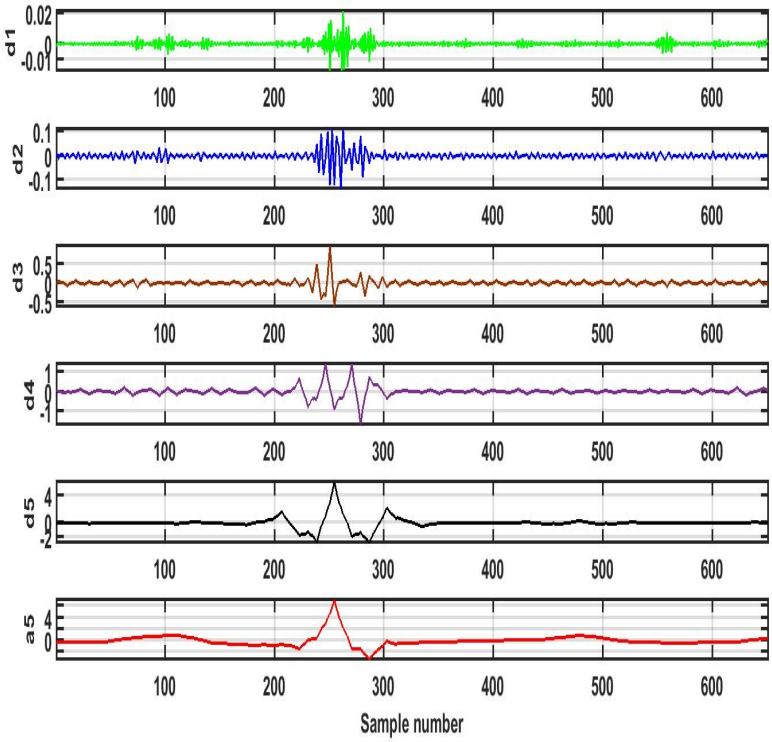

Figure 14: SBs of normal ECG signal (Dataset-B).

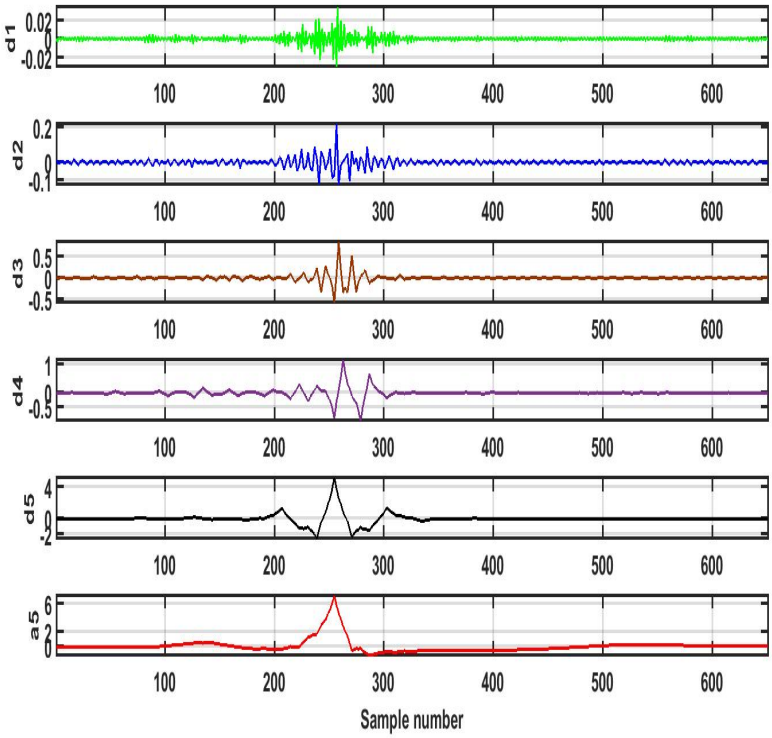

Figure 15: SBs of MI ECG signal (Dataset-B).

6.7. Features used

In order to differentiate normal and MI ECG signals, we have extracted entropy based features namely RE, SFD and FE from the six subbands obtained after the wavelet decomposition. Hence total 18 features are derived for each dataset (Dataset-A and Dataset-B). For detailed information about the entropy based features, one may refer [54].

6.7.1. Renyi Entropy (RE)

Renyi entropy (RE) generalizes the Shanon entropy, the collision entropy, the Hartley entropy and the min entropy. Entropies quantify the uncertainty, diversity, and randomness of the signal [55]. The RE of the signal can be defined as:

$$E_{RE}(X) = \frac{1}{\beta - 1} log\Big(\sum_{n=1}^{x} E_n^{\beta}\Big) \qquad \text{for } \beta \neq 1 \tag{27}$$

Here, X is a random variable with possible outcomes $1, 2, ..., x$ and E_n is the corresponding probabilities for $n \in 1, 2, ..., x$. β is the order of renyi entropy, we have taken $\beta = 2$. So, we can say that the RE is negative of the logarithm of energy.

6.7.2. Signal Fractal Dimension (SFD)

It is a ratio that provides the statistical index by comparing the change in detail of a pattern with the scale at which it is measured [56]. It can also be understood as a measure of the area filling capacity of a pattern that specifies how the fractal scales vary from the area it is embedded in [57]. Mathematically, SFD can be defined as:

$$\text{FD} = \frac{log(M_r)}{log(\frac{1}{r})} \tag{28}$$

M_r specifies the number of self-similar patterns used to fill the original pattern and r is the ratio used to decompose the original pattern into M_r self-similar patterns.

6.7.3. Fuzzy Entropy (FE)

FE logic is based on fuzzy sets. In this approach, every element has some degree of membership to the fuzzy set and FE is defined as the fuzziness of those fuzzy sets[58, 59]. Further details can be found in [60, 61, 54] Mathematically, it can be evaluated as:

$$\Psi^l(G, w) = \frac{1}{D-l} \sum_{x=1}^{D-l} \frac{1}{D-l-1} \Big[\sum_{y=1, y \neq x}^{D-l} (D_{xy}^l) \Big] \tag{29}$$

For evaluating FE, sequences of length l are extracted from the ECG signals, x and y are two such sequences. $D^l(x, y)$ denotes the degree of similarity between the sequences x and y. w and G denotes the width and the gradient of the threshold of fuzzy similarity, respectively.

6.8. Feature extraction and evaluation

We have extracted eighteen discriminating features using RE, SFD and FE. Student's t-test [20] is performed on the computed features to obtain the t-values and to evaluate the significance of the features and to reduce redundancy. If t-value is closer to 0 for a feature than it is not considered a good distinguishing feature and a t-value greater than 2 suggests that the feature is significant with greater than 95% confidence. The t-values are also used for ranking the features. The t-value for a feature can be calculated by :

$$t = \frac{\mu_x - \mu_y}{\sqrt{\frac{var_x}{n} + \frac{var_y}{m}}} \tag{30}$$

Here, x and y are sequences of feature values obtained for normal and MI affected ECG, respectively. μ_x and μ_y denotes the mean of the sequences x and y, respectively; var_x and var_y are the variances of the sequences x and y, respectively. While, n and m are the size of the sequences x and y, respectively.

Tables 2, 3 and 4 shows the statistical results and ranks of the derived features extracted from Dataset-B whereas Tables 5, 6 and 7 shows the statistical results and ranks of the derived features extracted from the Dataset-A . We can see from the tables that all the derived features have t-values much greater than 0, thus they all can be considered as good discriminating features.

Table 2: Statistical analysis (mean±standard–deviation, t-value) and rank of FE features extracted from Dataset-B.

SBs	**FE**			
	Normal	MI	t-value	Rank
1	0.036601±0.00557	0.035714±0.008357	12.964	16
2	0.00854±0.00525	0.012772±0.006782	68.999	9
3	0.056829±0.038824	0.093433±0.050868	80.389	7
4	0.059449±0.035633	0.098532±0.049697	91.644	5
5	0.058194±0.01934	0.079466±0.0367052	80.984	6
6	0.067571±0.006693	0.067067±0.008467	6.49	18

Table 3: Statistical analysis (mean±standard–deviation, t-value) and rank of SFD features extracted from Dataset-B.

SBs	**SFD**			
	Normal	MI	t-value	Rank
1	1.079823±0.006082	1.08285±0.008563	41.545	12
2	2.048694±0.023434	2.055454±0.023727	26.297	15
3	1.982372±0.024394	1.980440±0.025977	7.136	17
4	1.749132±0.056587	1.722266±0.047880	44.733	10
5	1.322204±0.022021	1.333103±0.023757	44.483	11
6	1.171512±0.008276	1.174499±0.010771	30.840	14

Table 4: Statistical analysis (mean±standard–deviation, t-value) and rank of RE features extracted from Dataset-B.

SBs	**RE**			
	Normal	MI	t-value	Rank
1	-11.96884±0.216748	-11.876987±0.30642	35.248	13
2	-0.54794±1.082699	-1.77337±1.028948	104.503	2
3	-3.611582±1.07665	-4.79544±1.043250	101.143	3
4	-5.937204±0.77131	-6.903166±0.84793	112.059	1
5	-7.668099±0.602839	-8.340237±0.789576	95.078	4
6	-10.281933±0.28111	-9.994589±0.575838	72.414	8

Table 5: Statistical analysis (mean±standard–deviation, t-value) and rank of FE features extracted from Dataset-A.

SBs	**FE**			
	Normal	MI	t-value	Rank
1	0.035033±0.006651	0.03272±0.010304	27.899	15
2	0.042126±0.027990	0.085840±0.044800	124.022	4
3	0.083349±0.054992	0.167719±0.0819512	125.219	3
4	0.060826±0.035952	0.106215±0.057164	100.519	6
5	0.057571±0.018058	0.08141±0.03706	93.423	7
6	0.067042±0.006432	0.065443±0.00993	20.015	16

Table 6: Statistical analysis (mean±standard–deviation, t-value) and ranking of SFD features extracted from Dataset-A.

SBs	**SFD**			
	Normal	MI	t-value	Rank
1	1.079696±0.0061147	1.0823648±0.0094650	35.106	14
2	2.0514947±0.0181836	2.0697017±0.0290163	79.608	9
3	1.9811342±0.0142314	1.9784563±0.0171049	16.454	17
4	1.7545415±0.0549683	1.7302318±0.0477141	41.498	12
5	1.3222345±0.0220341	1.3347350±0.0237904	50.980	11
6	1.1715140±0.0082802	1.1753004±0.0107062	39.149	13

Table 7: Statistical analysis (mean±standard–deviation, t-value) and rank of RE features extracted from Dataset-A.

SBs	**RE**			
	Normal	MI	t-value	Rank
1	-12.010487±0.2176387	-11.99313±0.3086413	6.622	18
2	-3.2885872±1.1153335	-4.8984011±1.1525053	130.999	1
3	-4.4976935±1.0200455	-5.9443851±1.1103738	127.203	2
4	-5.9291837±0.7737577	-6.8541227±0.9809068	102.951	5
5	-7.6147460±0.6138808	-8.1856552±0.8687662	77.321	10
6	-10.228075±0.3101275	-9.8010275±0.7326815	90.070	8

6.9. Classification and Performance Evaluation

The work in this paper uses k-nearest neighbours (KNN)[62] for classification. KNN is a non-parametric instance based algorithm which can be used for both classification and regression ML problems [63]. This algorithm, when employed on classification problems, makes the prediction based on the distance from the k neighbours nearest to the particular sample[62, 64]. Hence, finding the optimal k is very crucial for achieving the highest performance. For finding optimal k, elbow method and silhouette score analysis are employed [65]. The distance metric chosen for the classification is Euclidean[62]. This algorithm is cost-effective and doesn't require high computational power unlike other ML algorithms like support vector machine (SVM) and deep learning methods[66]. For cross-validation, we have used a 10-fold CV method which is one of the most preferred and robust tools for model validation and eliminating the over-fitting[67]. In this method, the original data has been split into ten equal groups of 5072 epochs. Out of 10 groups, 9 groups (45656 epochs) have been used for training and one subgroup (5072 epochs) has been employed for the validation. The process is iterated ten times by considering each subgroup for the validation. The average of the validations is considered as the actual performance of the system.

7. Results

In this work, we have performed the classification of normal ECG signals from MI ECG signals using the *Physikalisch-Technische Bundesanstalt* diagnostic ECG database [21].The dataset consists of 50728 ECG epochs taken from 200 subjects, of whom 149 are male subjects and 51 female subjects. The experiments and simulations were performed on Intel Xeon 3.5 GHz (E3–1245) processor with 16 GB RAM using MATLAB-9. The process of classifying MI ECG signals took only 21.5 seconds to complete (including both model-training and model-validation) on both clean and noisy datasets. In this case, we have performed decomposition up to 5 levels, and have extracted the features namely

FE, FD and RE. We were able to achieve an ACC of 99.74% using Dataset-A and an ACC of 99.62% on the Dataset-B with 10-fold CV using KNN as the classifier. The K-fold CV is a preferred tool for the purpose of model validation as it takes into account the overfitting of a model. Tables 8 and 9 shows the confusion matrix obtained for classification done on Dataset-B and Dataset-A, here here PPV stands for positive predictive value. The performance characteristics of the classification performed on the Dataset-A are shown in Table 10 and performance characteristics of the classification performed on the Dataset-B are shown in Table 11. Fig. 16 shows the ROC curves for the classification of both datasets. The area under curve (AUC) of receiver operating characteristics (ROC) obtained for both type of signals (with or without noise) is 1.00.

Fig. 17 and 18 depict the variation of classification accuracy for different combination of features for datasets A and B, respectively. Table 12 depicts the best classification accuracy(%) for various classifiers.

Table 8: Confusion matrix obtained for of MI ECG signal using Dataset-A across 10 fold with KNN.

		Predicted Class				
		Normal	MI	SEN(%)	SPE(%)	PPV(%)
True	Normal	10477 (20.66%)	69 (0.13%)	99.12	99.76	99.07
Class	MI	64 (0.12%)	40118(79.09%)	99.76	99.12	99.77

Table 9: Confusion matrix obtained for ECG signal using Dataset-B across 10 fold with KNN.

		Predicted Class				
		Normal	MI	SEN(%)	SPE(%)	PPV(%)
True	Normal	10453 (20.61%)	93 (0.18%)	99.35	99.84	99.39
Class	MI	98 (0.19%)	40084(79.02%)	99.84	99.35	99.83

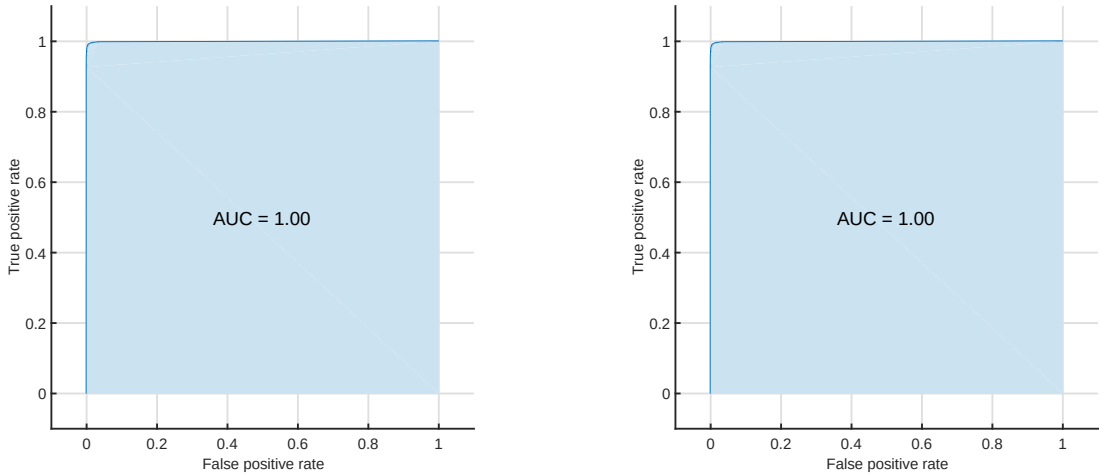

(a) Dataset-A (b) Dataset-B

Figure 16: ROCs for MI ECG classification.

Table 10: Classification performance for dataset-B with best classifier (KNN).

Algorithm	**ACC(%)**	**SEN(%)**	**SPE(%)**	**PPV(%)**	**AUC**	**F1 Score**
KNN	99.74	99.84	99.35	99.83	1.00	0.9983

Table 11: Classification performance for dataset-A with best classifier (KNN).

Algorithm	**ACC(%)**	**SEN(%)**	**SPE(%)**	**PPV(%)**	**AUC**	**F1 Score**
KNN	99.62	99.76	99.12	99.77	1.00	0.9976

Table 12: Classification obtained using different classifiers.

Classifier	Dataset-A	Dataset-B
Complex trees	95.3 %	95.7%
Quadratic SVM	94.8%	96.8%
Cubic SVM	99.1%	99.3%
Bagged trees	99.1%	99.0%
KNN	**99.64**%	**99.72**%

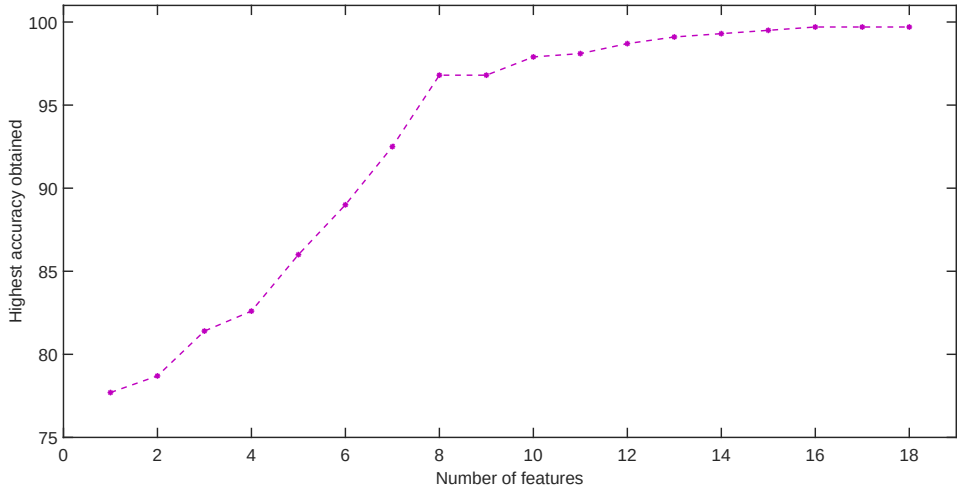

Figure 17: ACC (%) versus NoF for Dataset-A.

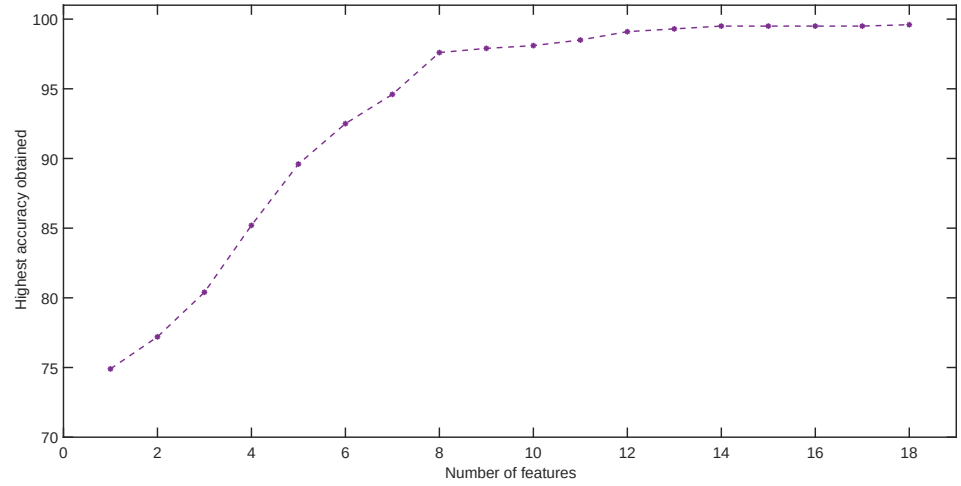

Figure 18: ACC (%) versus NoF for Dataset-B.

8. Discussions

The salient features of the developed system are given below:

1. Our proposed model performed well for both noisy and clean ECG signals.

2. AUC of ROC obtained both datasets is equal to unity which is the maximum value attainable for any model.
3. We have achieved the highest ACC of 99.74% and F1-score 0.998. The ACC as well as F1 score have been found superior than earlier state-of-the-art MI CAD systems (Table 13) using the same *Physikalisch-Technische Bundesanstalt* ECG database.
4. The method involves the use of a new class of biorthogonal symmetric FB.
5. The model involves the use of only single channel and single lead ECG signals. Many methods [11, 15, 17, 68] have used multiple leads which makes their method complex for deploying in practical applications.
6. The method uses only 651 samples of ECG beats which are sampled at a sampling rate of 1000 Hz thus reducing the wavelet processing time.
7. The methods described in [13, 69] achieved 98.8% accuracy and 99.3% accuracy, respectively. However, both the methods involves the use of large NoF. The proposed algorithm requires the use of only 18 discriminating features which reduces the computational cost required and makes the model cost-effective.
8. Kumar et al [69] used analytical time frequency wavelet transform (ATFWT) which is a complex and redundant transform. However, we have used critically sampled biorthogonal wavelet transform which is computationally complex than ATFWT.
9. The proposed methods took only 1.35 seconds for the extraction of all the 18 features for a single ECG signal.
10. The model is validated using 10-fold CV technique to mitigate chances of over-fitting and to increase the robustness of the model.
11. The work was implemented on a computer with an Intel Xeon 3.5 GHz (E3–1245) processor and 16 GB RAM. The classification using KNN took 21.5 seconds to classify of 50728 ECG epochs employing 10-fold CV. Thus, the proposed technique can be considered computationally less demanding and fast, therefore, it may considered to deploy in hospitals and clinics.
12. Acharya et al.[8] have already used deep learning using CNN architecture on the database used in this study for automated detection of MI. We intend to try different deep neural network architectures on a bigger dataset to diagnose MI, as our future work. Recently few new deep earning techniques have been investigated for the physiological signals [70] . It would be interesting to use the proposed wavelet as a wavelet sequence in a deep neural network to detect MI ECG signals. Also, our technique can also be employed to detect the coronary artery disease, early stage of MI and also congestive heart failure.

Table 13: Various MI detection CAD systems and their comparison.

Study (Year)	**Technique**	**Performance-measure**
Lahiri et al. [7], 2009	**No. of ECG signals :** • 64,680 R-peaks from 1,848 **Features:** • Detection of R-peaks • Phase space SFD of ECG **Classifiers:** • Artificial neural network	ACC=90%
Jayachandran et al. [71], 2010	**No. of ECG beats** • Normal: 2282 • MI:718 **Features:** • DWT based entropy	ACC=96.93%
Arif et al. [15], 2012	**No. of ECG signals** • Normal: 3200 • MI: 16960 **Features:** • QRS detection • Time-domain features **Classifiers:** • k-nearest neighbor	SEN=99.97% SPE=99.90%
Sun et al. [18], 2012	**No. of ECG signals :** • Normal: 79 records • MI: 369 records **Features:** • ST detection • Multiple instance learning **Classifiers:** • Support vector machine	SEN=92.60% SPE=82.40%
Banerjee et al. [68], 2014	**No. of ECG signals :** • Normal: 10546 • MI: 40182	

Reference (Year)	Methodology	Performance
	Features: • XWT Based Method • Employed the use of 3 leads **Classifiers:** • Threshold Based Classifier	ACC=97.60%
Safdarian et al.[6], 2014	**No. of ECG signals :** • 549 records **Features:** • T-wave detection • Artificial neural network **Classifiers:** • Naïve Bayes	ACC=94.74%
Liu et al. [11], 2015	**No. of ECG signals :** • Normal: 52 subjects • MI: 148 patients **Features:** • R-peaks detection • ECG polynomial fitting (polyfit) **Classifiers:** • Decision tree	ACC=94.40%
Sharma et al. [17], 2015	**No. of ECG signals :** 25 • 549 records **Features:** • Wavelet transform based multiscale energy • Multiscale eigenspace analysis **Classifiers:** • SVM	ACC=96.00% SEN=93.00% SPE=99.00%
Acharya et al. [13], 2016	**No. of ECG signals :** • Normal: 125652 • MI: 485,753 **Features:** • Detection of R-peaks	ACC=98.80%

Reference (Year)	Methodology	Performance
	• Detection using 47 features • Localization using 25 features **Classifiers:** • k-nearest neighbor	SEN=99.45% SPE=96.27%
Acharya et al. [8], 2017	**No. of ECG signals :** • Normal: 10,546 • MI: 40,182 **Features:** • Detection of R-peaks • Deep neural network **Classifiers:** • Convolutional neural network	**Dataset-A:** ACC=93.53% SEN=93.71% SPE=92.83% **Dataset-B:** ACC=95.22% SEN=95.49% SPE=94.19%
Kumar et al. [69], 2017	**No. of ECG signals :** • Normal: 10548 • MI: 40182 **Features:** • FAWT and SEnt • Employed the use of 1 lead **Classifiers:** • LS-SVM	ACC=99.31%
Proposed Method	**No. of ECG Signals:** • Normal: 10,546 • MI: 40,182 **Features:** • RE, FE and SFD • employed 10-fold CV • cost-effective and reliable • Denoising not required **Classifiers:** • k-nearest neighbor	**Dataset-B:** ACC=99.74% SEN=99.84% SPE=99.35% **Dataset-A:** ACC=99.62% SEN=99.76% SPE=99.12%

9. Conclusion

In this study, we have developed an automated system for the classification of MI and normal ECG signals using a single-channel ECG database and a novel class of OBWFB with a few features. The KNN classifier has been employed to classify of both noisy and clean MI ECG signals. For the mitigation of overfitting and to ensure robustness of the model, 10–fold CV was used for obtaining the results. Wavelet-based FE, SFD, and RE features have been extracted. For feature ranking, we have performed Student's t-test. The system developed is cost-effective and has produced high accuracies of 99.74% and 99.62% for the Dataset-B (clean) and Dataset-A (noisy), respectively. This will speed-up the diagnosis and will give both the patient and the hospital cost benefits for health services. The wavelet-based features obtained from the designed OBWFB have been found to be excellent in identifying MI in human beings. We have thus presented an automated system for detection of MI which is robust, accurate and cost-effective. The proposed CAD thus may be deployed in real-time practical setup for monitoring, diagnosis and treatment of MI to reduce time, cost and medical competence.

The suggested automatic diagnosis system for MI is a non-invasive approach for MI detection and will help in the triage of patients presenting with suspicious symptoms. This design can be easily implemented in both urban and rural areas, due to its low cost and user-friendly system. This methodology can be further used for the detection of other cardiac as well as neurological disorders which are difficult to diagnose like arrhythmia [72], dementia, sleep apnea, etc. using ECG and electroencephalogram signals [73].

References

[1] U. R. Acharya, N. Kannathal, L. M. Hua, L. M. Yi, Study of heart rate variability signals at sitting and lying postures, Journal of bodywork and Movement Therapies 9 (2) (2005) 134–141.

[2] D. Kulick, D. Lee, Heart attack (myocardial infarction), Accessed October 6 (2008) 2013.

[3] D. Mozaffarian, E. J. Benjamin, A. S. Go, D. K. Arnett, M. J. Blaha, M. Cushman, S. R. Das, S. de Ferranti, J.-P. Després, H. J. Fullerton, et al., Heart disease and stroke statistics-2016 update: a report from the american heart association, Circulation 133 (4) (2016) e38–e360.

[4] J. L. Garvey, ECG techniques and technologies, Emergency Medicine Clinics 24 (1) (2006) 209–225.

[5] R. Acharya, S. M. Krishnan, J. A. Spaan, J. S. Suri, Advances in cardiac signal processing, Springer, 2007.

[6] N. Safdarian, N. J. Dabanloo, G. Attarodi, A new pattern recognition method for detection and localization of myocardial infarction using t-wave integral and total integral as extracted features from one cycle of ecg signal, Journal of Biomedical Science and Engineering 7 (10) (2014) 818.

[7] T. Lahiri, U. Kumar, H. Mishra, S. Sarkar, A. D. Roy, Analysis of ecg signal by chaos principle to help automatic diagnosis of myocardial infarction.

[8] U. R. Acharya, H. Fujita, S. L. Oh, Y. Hagiwara, J. H. Tan, M. Adam, Application of deep convolutional neural network for automated detection of myocardial infarction using ecg signals, Information Sciences 415 (2017) 190–198.

[9] P. De Chazal, C. Heneghan, E. Sheridan, R. Reilly, P. Nolan, M. O'Malley, Automatic classification of sleep apnea epochs using the electrocardiogram, in: Computers in Cardiology 2000, IEEE, 2000, pp. 745–748.

[10] L. Chen, X. Zhang, C. Song, An automatic screening approach for obstructive sleep apnea diagnosis based on single-lead electrocardiogram, IEEE Transactions on Automation Science and Engineering 12 (1) (2015) 106–115.

[11] B. Liu, J. Liu, G. Wang, K. Huang, F. Li, Y. Zheng, Y. Luo, F. Zhou, A novel electrocardiogram parameterization algorithm and its application in myocardial infarction detection, Computers in biology and medicine 61 (2015) 178–184.

[12] U. R. Acharya, H. Fujita, M. Adam, S. L. Oh, K. V. Sudarshan, J.-H. Tan, J. E. W. Koh, Y. Hagiwara, C. K. Chua, C. K. Poo, R. S. Tan, Automated characterization and classification of coronary artery disease and myocardial infarction by decomposition of ecg signals: A comparative study, Inf. Sci. 377 (2017) 17–29.

[13] U. R. Acharya, H. Fujita, M. Adam, O. S. Lih, T. J. Hong, V. K. Sudarshan, J. E. Koh, Automated characterization of arrhythmias using nonlinear features from tachycardia ecg beats, in: Systems, Man, and Cybernetics (SMC), 2016 IEEE International Conference on, IEEE, 2016, pp. 000533–000538.

[14] U. R. Acharya, H. Fujita, K. V. Sudarshan, S. L. Oh, M. Adam, J.-H. Tan, J. H. Koo, A. Jain, C. M. Lim, C. K. Chua, Automated characterization of coronary artery disease, myocardial infarction, and congestive heart failure using contourlet and shearlet transforms of electrocardiogram signal, Knowl.-Based Syst. 132 (2017) 156–166.

[15] M. Arif, I. A. Malagore, F. A. Afsar, Detection and localization of myocardial infarction using k-nearest neighbor classifier, Journal of medical systems 36 (1) (2012) 279–289.

[16] S. Banerjee, M. Mitra, Cross wavelet transform based analysis of electrocardiogram signals, International Journal of Electrical, Electronics and Computer Engineering 1 (2) (2012) 88–92.

[17] L. Sharma, R. Tripathy, S. Dandapat, Multiscale energy and eigenspace approach to detection and localization of myocardial infarction, IEEE transactions on biomedical engineering 62 (7) (2015) 1827–1837.

[18] L. Sun, Y. Lu, K. Yang, S. Li, Ecg analysis using multiple instance learning for myocardial infarction detection, IEEE transactions on biomedical engineering 59 (12) (2012) 3348–3356.

[19] P. Vaidyanathan, T. Nguyen, A 'trick' for the design of fir half-band filters, Circuits and Systems, IEEE Transactions on 34 (3) (1987) 297–300. doi:10.1109/TCS.1987.1086124.

[20] Student, The probable error of a mean, Biometrika (1908) 1–25.

[21] M. Je, M. Gb, P. Ck, Goldberger al, amaral lan, glass l, hausdorff jm, ivanov pch, mark rg, mietus je, moody gb, peng ck, stanley he. physiobank, physiotoolkit, and physionet: Components of a new research resource for complex physiologic signals, vol 101 220.

[22] B. N. Singh, A. K. Tiwari, Optimal selection of wavelet basis function applied to ecg signal denoising, Digital signal processing 16 (3) (2006) 275–287.

[23] J. Pan, W. J. Tompkins, A real-time qrs detection algorithm, IEEE transactions on biomedical engineering (3) (1985) 230–236.

[24] G. Strang, T. Nguyen, Wavelets and filter banks, Wellesley-Cambridge Press, 1997.

[25] M. Sharma, D. Goyal, P. Achuth, U. R. Acharya, An accurate sleep stages classification system using a new class of optimally time-frequency localized three-band wavelet filter bank, Computers in Biology and Medicine 98 (2018) 58 – 75. doi:https://doi.org/10.1016/j.compbiomed.2018.04.025.
URL http://www.sciencedirect.com/science/article/pii/S0010482518301069

[26] M. Sharma, S. Agarwal, U. R. Acharya, Application of an optimal class of antisymmetric wavelet filter banks for obstructive sleep apnea diagnosis using ecg signals, Computers in Biology and Medicine 100 (2018) 100 – 113. doi:https://doi.org/10.1016/j.compbiomed.2018.06.011.
URL http://www.sciencedirect.com/science/article/pii/S0010482518301598

[27] M. Sharma, P. V. Achuth, R. B. Pachori, V. M. Gadre, A parametrization technique to design joint time–frequency optimized discrete-time biorthogonal wavelet bases, Signal Processing 135 (2017) 107 – 120.

[28] M. Sharma, A. Dhere, R. B. Pachori, V. M. Gadre, Optimal duration-bandwidth localized antisymmetric biorthogonal wavelet filters, Signal Processing 134 (2017) 87 – 99.

[29] M. Sharma, R. B. Pachori, U. R. Acharya, A new approach to characterize epileptic seizures using analytic time-frequency flexible wavelet transform and fractal dimension, Pattern Recognition Letters 94 (2017) 172 – 179. doi:https://doi.org/10.1016/j.patrec.2017.03.023.
URL http://www.sciencedirect.com/science/article/pii/S0167865517300995

[30] M. Sharma, D. Bhati, S. Pillai, R. B. Pachori, V. M. Gadre, Design of time–frequency localized filter banks: Transforming non-convex problem into convex via semidefinite relaxation technique, Circuits, Systems, and Signal Processing 35 (10) (2016) 3716–3733.

[31] M. Sharma, D. Deb, U. R. Acharya, A novel three-band orthogonal wavelet filter bank method for an automated identification of alcoholic eeg signals, Applied Intelligencedoi:10.1007/s10489-017-1042-9.
URL https://doi.org/10.1007/s10489-017-1042-9

[32] D. Bhati, M. Sharma, R. B. Pachori, V. M. Gadre, Time-frequency localized three-band biorthogonal wavelet filter bank using semidefinite relaxation and nonlinear least squares with epileptic seizure EEG signal classification, Digital Signal Processing 62 (2017) 259 – 273.

[33] M. Sharma, R. B. Pachori, A novel approach to detect epileptic seizures using a combination of tunable-q wavelet transform and fractal dimension, Journal of Mechanics in Medicine and Biology 0 (0) (0) 1740003. arXiv:http://www.worldscientific.com/doi/pdf/10.1142/S0219519417400036, doi:10.1142/S0219519417400036.
URL http://www.worldscientific.com/doi/abs/10.1142/S0219519417400036

[34] T. Cooklev, A. Nishihara, M. Sablatash, Regular orthonormal and biorthogonal wavelet filters, Signal Process 57 (2) (1997) 121–137.

[35] B. Patil, P. Patwardhan, V. Gadre, Eigenfilter approach to the design of one-dimensional and multidimensional two-channel linear-phase FIR perfect reconstruction filter banks, IEEE Trans. Circ. Sys. I 55 (11) (2008) 3542–3551.

[36] M. Sharma, V. M. Gadre, S. Porwal, An eigenfilter-based approach to the design of time-frequency localization optimized two-channel linear phase biorthogonal filter banks, Circ. Syst. and Signal Process. 34 (3) (2015) 931–959.

[37] S.-M. Phoong, C. Kim, P. Vaidyanathan, R. Ansari, A new class of two-channel biorthogonal filter banks and wavelet bases, Signal Processing, IEEE Transactions on 43 (3) (1995) 649–665. doi:10.1109/78.370620.

[38] C. Kim, R. Ansari, FIR/IIR exact reconstruction filter banks with applications to subband coding of images, in: Circuits and Systems, 1991., Proceedings of the 34th Midwest Symposium on, 1991, pp. 227–230 vol.1. doi:10.1109/MWSCAS.1991.252057.

[39] M. Shensa, The discrete wavelet transform: wedding the a trous and mallat algorithms, Signal Processing, IEEE Transactions on 40 (10) (1992) 2464–2482. doi:10.1109/78.157290.

[40] R. Wilson, G. H. Granlund, The uncertainty principle in image processing, ieee trans. pattern anal, Mach. Intell. PAMI- 6 (6) (1984) 758–767.

[41] Y. Dandach, P. Siohan, Design method of OFDM/OQAM systems using a weighted time frequency localization criterion, in: 18th european signal processing conference 2010.

[42] D. Monro, B. G. Sherlock, Space-frequency balance in biorthogonal wavelets, In: Int 1997 (1997) 624–627.

[43] D. Tay, Two-stage, least squares design of biorthogonal filter banks, Vision, Image and Signal Processing, IEE Proceedings - 149 (6) (2002) 341–346. doi:10.1049/ip-vis:20020654.

[44] D. B. Tay, Balanced-uncertainty optimized wavelet filters with prescribed vanishing moments, Circ. Syst. and Signal Process 23 (2) (2004) 105–121.

[45] A. Baradarani, Q. J. Wu, M. Ahmadi, P. Mendapara, Tunable halfband-pair wavelet filter banks and application to multifocus image fusion, Pattern Recognition 45 (2) (2012) 657–671.

[46] R. Ansari, C. Kim, M. Dedovic, Structure and design of two-channel filter banks derived from a triplet of halfband filters, Circuits and Systems II: Analog and Digital Signal Processing, IEEE Transactions on 46 (12) (1999) 1487–1496. doi:10.1109/82.809534.

[47] D. Tay, M. Palaniswami, A novel approach to the design of the class of triplet halfband filterbanks, Circuits and Systems II: Express Briefs, IEEE Transactions on 51 (7) (2004) 378–383. doi:10.1109/TCSII.2004.831430.

[48] H. Kha, H. Tuan, T. Nguyen, Optimal design of fir triplet halfband filter bank and application in image coding, Image Processing, IEEE Transactions on 20 (2) (2011) 586–591. doi:10.1109/TIP.2010.2059450.

[49] R. Ishii, K. Furukawa, The uncertainty principle in discrete signals, ieee trans, Circ. Syst. 33 (10) (1986) 1032–1034.

[50] R. Fischer, M. Akay, Fractal analysis of heart rate variability, Time Frequency and Wavelets in Biomedical Signal Processing (1998) 719–28.

[51] M. Sharma, A. Dhere, R. B. Pachori, U. R. Acharya, An automatic detection of focal EEG signals using new class of time–frequency localized orthogonal wavelet filter banks, Knowledge-Based Systems 118 (2017) 217 – 227.

[52] T. Kalayci, O. Ozdamar, Wavelet preprocessing for automated neural network detection of eeg spikes, IEEE engineering in medicine and biology magazine 14 (2) (1995) 160–166.

[53] P. Jahankhani, V. Kodogiannis, K. Revett, Eeg signal classification using wavelet feature extraction and neural networks, in: Modern Computing, 2006. JVA'06. IEEE John Vincent Atanasoff 2006 International Symposium on, IEEE, 2006, pp. 120–124.

[54] U. R. Acharya, Y. Hagiwara, J. E. W. Koh, S. L. Oh, J. H. Tan, M. Adam, R. San Tan, Entropies for automated detection of coronary artery disease using ecg signals: A review, Biocybernetics and Biomedical Engineering.

[55] D. E. Lake, Renyi entropy measures of heart rate gaussianity, IEEE Transactions on Biomedical Engineering 53 (1) (2006) 21–27. doi:10.1109/TBME.2005.859782.

[56] J. h. Zhou, O. Sourina, A new research on the application of fractal dimension, in: 2008 International Conference on Advanced Computer Theory and Engineering, 2008, pp. 138–142. doi:10.1109/ICACTE.2008.213.

[57] C. C. Chen, J. S. DaPonte, M. D. Fox, Fractal feature analysis and classification in medical imaging, IEEE Transactions on Medical Imaging 8 (2) (1989) 133–142. doi:10.1109/42.24861.

[58] L. Zadeh, Fuzzy sets, Information and Control 8 (3) (1965) 338 – 353.

[59] W. Chen, Z. Wang, H. Xie, W. Yu, Characterization of surface emg signal based on fuzzy entropy, IEEE Transactions on neural systems and rehabilitation engineering 15 (2) (2007) 266–272.

[60] U. R. Acharya, F. Molinari, S. V. Sree, S. Chattopadhyay, K.-H. Ng, J. S. Suri, Automated diagnosis of epileptic eeg using entropies, Biomedical Signal Processing and Control 7 (4) (2012) 401–408.

[61] H. L. Lu, K. Ong, P. Chia, An automated ecg classification system based on a neuro-fuzzy system, in: Computers in Cardiology 2000. Vol.27 (Cat. 00CH37163), 2000, pp. 387–390. doi:10.1109/CIC.2000.898538.

[62] S. A. Dudani, The distance-weighted k-nearest-neighbor rule, IEEE Transactions on Systems, Man, and Cybernetics (4) (1976) 325–327.

[63] J. M. Keller, M. R. Gray, J. A. Givens, A fuzzy k-nearest neighbor algorithm, IEEE transactions on systems, man, and cybernetics (4) (1985) 580–585.

[64] L. E. Peterson, K-nearest neighbor, Scholarpedia 4 (2) (2009) 1883.

[65] P. Cunningham, S. J. Delany, k-nearest neighbour classifiers, Multiple Classifier Systems 34 (2007) 1–17.

[66] Y. Liao, V. R. Vemuri, Use of k-nearest neighbor classifier, Computers & security 21 (5) (2002) 439–448.

[67] P. Refaeilzadeh, L. Tang, H. Liu, Cross-validation, in: Encyclopedia of database systems, Springer, 2009, pp. 532–538.

[68] S. Banerjee, M. Mitra, Application of cross wavelet transform for ecg pattern analysis and classification, IEEE transactions on instrumentation and measurement 63 (2) (2014) 326–333.

[69] M. Kumar, R. B. Pachori, U. R. Acharya, Automated diagnosis of myocardial infarction ecg signals using sample entropy in flexible analytic wavelet transform framework, Entropy 19 (9) (2017) 488.

[70] O. Faust, Y. Hagiwara, T. J. Hong, O. S. Lih, U. R. Acharya, Deep learning for healthcare applications based on physiological signals: a review, Computer Methods and Programs in Biomedicine.

[71] E. Jayachandran, et al., Analysis of myocardial infarction using discrete wavelet transform, Journal of medical systems 34 (6) (2010) 985–992.

[72] U. R. Acharya, H. Fujita, O. S. Lih, Y. Hagiwara, J. H. Tan, M. Adam, Automated detection of arrhythmias using different intervals of tachycardia ECG segments with convolutional neural network, Information Sciences 405 (2017) 81 – 90.

[73] U. R. Acharya, S. L. Oh, Y. Hagiwara, J. H. Tan, H. Adeli, Deep convolutional neural network for the automated detection and diagnosis of seizure using eeg signals, Computers in biology and medicine.